Carbon Letters (2022) 32:835–848
https://doi.org/10.1007/s42823-022-00318-w

Online ISSN 2233-4998
Print ISSN 1976-4251

ORIGINAL ARTICLE

In situ formed nano-Ni catalytic effect on graphitization of phenolic resin (thermodynamic and microstructure investigation)

H. Rastegar[1] · E. Mansorizadeh[1]

Received: 6 December 2021 / Revised: 29 December 2021 / Accepted: 7 January 2022 / Published online: 25 January 2022

Abstract
In the present study, the effect of nickel nitrate addition as a catalytic precursor for the in situ formation of Ni nanoparticles during the heating process has been investigated on the modification of microstructure and graphitization of amorphous carbon resulting from pyrolysis of phenolic resin. For this purpose, the prepared resin samples were cured in carbon substrate with and without additives at temperatures of 800, 1000, and 1250 °C. XRD, FESEM, and TEM studies were performed to investigate the phase and microstructural changes in the samples during the heating process. In addition to phase and microstructural studies, thermodynamic calculations of the reactions performed for the in situ formation of nickel nanoparticles and their effective factors during the curing process were performed. The results indicated that nickel nitrate is transformed to nickel nanoparticles of different sizes during the reduction process in a reduced atmosphere. The in situ formation of nickel nanoparticles and its catalytic effect led to the graphitization of carbon resulting from the pyrolysis of phenolic resin at a temperature of 800 °C and above. By increasing temperature, the morphology of the formed graphite changed and hollow carbon nanotubes, carbon cells, and onion skin carbon were formed in the microstructure. It was also observed that by increasing the temperature and the amount of additive, carbon nanotubes and their size are increased. A noteworthy point from thermodynamic calculations during the formation of nickel nanoparticles was that the nickel nanoparticles themselves acted as accelerators of nickel oxide reduction reactions and the formation of nickel nanoparticles. This increases the amount of amorphous carbon graphitization resulting from the pyrolysis of phenolic resin which leads to the formation of more carbon nanotubes at higher temperatures.

Keywords In situ nano-Ni · Catalytic graphitization · Carbon nanotubes (CNTs) · Phenolic resin · Thermodynamic investigation

1 Introduction

One of the main applications of phenolic resins is their use as a binder in carbon-containing refractory materials [1–5]. The resin pyrolysis process occurs during heating of refractories containing phenolic resin. Pyrolysis is a process in which the resin undergoes dehydration, hydrogenation, decomposition to light hydrocarbons, and finally amorphous carbon is formed. The amorphous carbon has disadvantages such as poor oxidation resistance and high brittleness, and if it is possible to change this structure into graphite and crystalline carbon by controlling the formulation, sampling and curing process, these disadvantages will become advantages that can have a significant impact on refractories containing final carbon and finally on the quality of the resulting steel [6–9]. Much research has been performed to achieve this goal, the most important of which is the use of nano-catalytic additives that lead to the in situ formation of nanoparticles, the most important of which include Fe, Ni, and Co, which eventually cause graphitization of amorphous carbon resulting from pyrolysis of phenolic resin and change the morphology of the structure [10–15]. Furthermore, previous research has shown that in addition to the effect of catalytic additives on graphitized amorphous carbon resulting from the pyrolysis of phenolic resin, the presence of catalytic nanoparticles improves the rate of some microstructural reactions in the matrix phase of carbon-containing refractories is increased during the curing process. Also, the morphology of the phases formed in the microstructure changes

✉ H. Rastegar
h.rastegar@srbiau.ac.ir; hosseinrastegar@gmail.com

[1] Department of Materials Science and Engineering, Saveh Branch, Islamic Azad University, Saveh, Iran

significantly from particular to fibrous after the curing process, which can improve the properties and increase the service life of the refractory material [16–18]. Of course, many parameters such as addition method, sample preparation process, curing conditions, additive percentage, etc. affect the quality of graphitization and microstructure morphology [19–21], based on which we refer to some relevant research.

Luz et al. [22] investigated changing the preparation process conditions (such as mixing, curing, and firing temperature), the use of two types of Novolac and Resole resin, and types of additives that can affect the graphitization of amorphous carbon. The result of their work reveled that Ferrocene is more effective in this phenomenon and the role of mixing and curing steps is very important so that the use of low energy mixing and slower curing increases the level of graphitization for samples at the same curing temperature.

In another study [23], the effect of nickel addition as a catalytic particle to phenolic resin was investigated. The results showed that amorphous carbon from pyrolysis of phenolic resin can be graphitized in the presence of nickel, where heating temperature has a greater effect on graphitization than other parameters.

Bitencourt et al. [24] also investigated the effect of various additives along with changes in the sampling process parameters on the graphitization of Novolac. The results of their study showed that graphitization of amorphous carbon resulting from pyrolysis of phenolic resin occurs with the presence of iron-containing additives (Ferrocene, Hematite, and Nano-Fe_2O_3) but the effect of Ferrocene is greater. Also, there is a possibility of agglomeration during sample preparation with the presence of nano-additives. Another important result obtained from this study on changing the sampling process parameters is that a heating rate of 3° per minute and 5 h stop at curing temperature of 1400 °C lead to the best results.

In another study [25], the role of in situ iron nanoparticles on the graphitization of carbon from pyrolysis of phenolic resin was investigated. The results showed that the graphitization temperature of amorphous carbon decreased by pyrolysis of phenolic resin and carbon nanoparticles were formed with onion skin and tubular morphology in microstructure. By increasing the curing temperature as well as the iron additive percentage, the amount and size of carbon nanotubes increases and also the oxidation resistance improves.

Based on the above, nickel nitrate was used in this study to obtain nickel nanoparticles in situ and to investigate their effect on carbon graphitization resulting from the pyrolysis of phenolic resin. Changes in curing temperatures as well as the percentage of nickel used in the composition were among the parameters considered in this study. Therefore, in the studies performed on the morphology and particle size of carbon structures, microstructural observations as well as relevant thermodynamic calculations for graphitization of amorphous carbon resulting from the pyrolysis of phenolic resin were pursued for the mechanism of graphite structure formation from amorphous carbon to be more controllable in this process and the relevant results be more accurate.

2 Experimental procedure

2.1 Preparation and pyrolysis of in situ nano-Ni containing phenolic resins

In this research, a type of Iranian phenolic resin (Novolac) with 55% constant carbon, MERCK nickel nitrate and ethanol were used as raw materials. To fabricate the samples, nickel nitrate was first weighed and added to ethanol and the resulting mixture was mixed using a magnetic stirrer at ambient temperature for 3 h and finally a uniform solution was prepared. Afterwards, phenolic resin (Novolac) was poured into the solution and stirred for homogenization for 2 h. The stirring operation was then continued at a temperature of 80 °C until the solvent was removed from the system and the resulting mixture became a uniform gel. After this step, the resulting gel was drained and placed at 24 °C for 24 h to remove volatiles. The final dried material was ground and passed through a mesh 80 sieve. The composition of the samples was adjusted so that the amount of nickel metal to resin was 0, 3, and 6 wt.% and was named PR, PRN-3, and PRN-6, respectively. Curing process of prepared samples was conducted in a reducing atmosphere (carbon media) at 800, 1000 and 1250 °C for 3 h. To evaluate and compare the properties, resin powders were prepared without additive and cured at 1200 °C according to the above curve.

2.2 Testing and characterization methods

X-ray diffraction (XRD) test was performed to investigate the phases formed in phenolic resin and the effect of nickel-containing additive on crystallization and graphitization of amorphous carbon resulting from pyrolysis of phenolic resin. To perform this test, CuKα beam irradiation with a wavelength of 1.5406 angstroms was used in an XRD device by Philips. The scanning step was considered 0.2 and X'Pert HighScore Plus software was used to interpret and identify the resulting peaks. Using this device, studies were performed to determine the Miller index of the formed crystallographic planes, the distance of the crystallographic planes, the size of the crystals and finally the percentage of graphitization in the resin samples. For this purpose, Eq. 1 (Scherrer equation) was used to calculate the size of the crystallites [26].

$$L_C = \frac{0.89\lambda}{\beta \cos\theta}. \quad (1)$$

In this equation, L_C is average crystallite size, 0.89 is shape factor, λ is the wavelength of X-ray, β denotes full width at half maximum of the (002) peak in radians, θ denotes the Braggs angle. After the L_C calculation degree of graphitization (G) was also determined by [27]:

$$G\% = \frac{0.344 - d_{002}}{0.344 - 0.3354}, \quad (2)$$

For the scanning electron microscopy studies, MIRA3 TESCAMield emission microscope was used for microstructural investigation of PR samples and TEMCM30 150 kV transmission electron microscope was used to study the morphology and microstructure of samples containing additives. Through this test, microstructural studies were performed with higher magnification and higher resolution. Also, diffraction patterns were taken from areas in the samples to study the crystallization and probable formation of graphite structure.

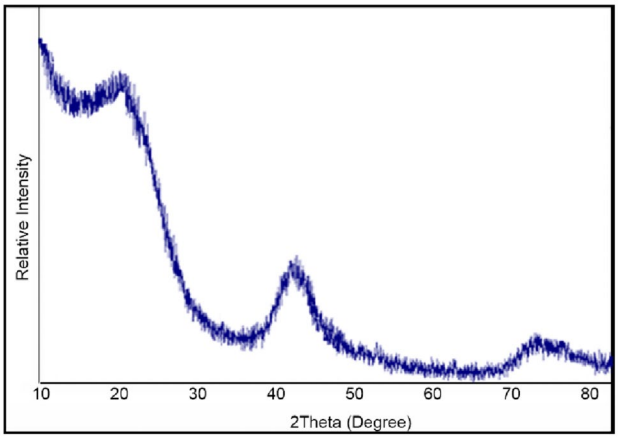

Fig. 1 XRD pattern of PR sample fired at 1200 ℃

3 Results and discussion

3.1 Phase evolution of different samples after pyrolysis

The X-ray diffraction pattern of the PR cured sample at 1200 °C is shown in Fig. 1. As can be seen, the diffraction pattern of the PR sample with no additives is quite amorphous as expected. Because after curing the PR sample, no crystalline structure is formed and amorphous or glassy carbon with low toughness and oxidation resistance is formed.

Figures 2 and 3 show the X-ray diffraction pattern of PRN-3 and PRN-6 samples cured at 800, 1000, and 1250 °C. As can be seen in these figures, the XRD pattern of PRN-3 and PRN-6 samples is completely different from the PR sample and a graphite crystal structure is formed in these samples. The peaks at 2θ angle of about 26° correspond to the (002) planes, 43° peaks correspond to the (100) planes, 54° peaks correspond to the (004) planes, and 78° peaks correspond to the (110) planes of graphite. With increasing temperature from 800 to 1250 °C and also with increasing the amount of nickel-containing additive in the amorphous carbon matrix, the intensity of carbon crystalline peaks increases and this indicates an increase in the amount of graphite crystal phase due to pyrolysis of phenolic resin.

Figures 4 and 5 show the effect of curing temperature on crystallite size (L_C) and graphitization percentage ($G\%$) of the samples PRN-3 and PRN-6, respectively. As shown in Figs. 4 and 5, using a nickel-containing additive in phenolic resin, the resin structure is closer to the graphite structure. That is, the distance of (002) planes in these compounds is closer to the distance of (002) planes of graphite (0.3354 nm) and also the length of formed crystals and the

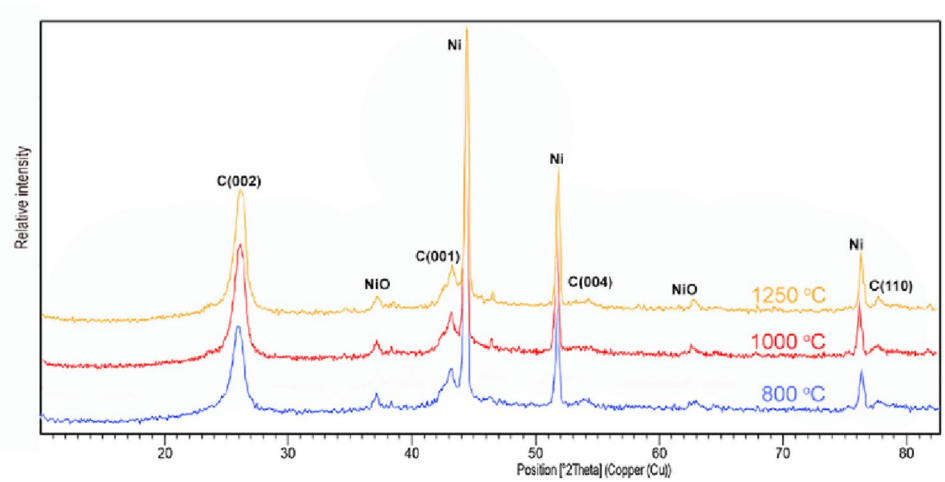

Fig. 2 XRD patterns of PRN-3 sample fired at different temperatures

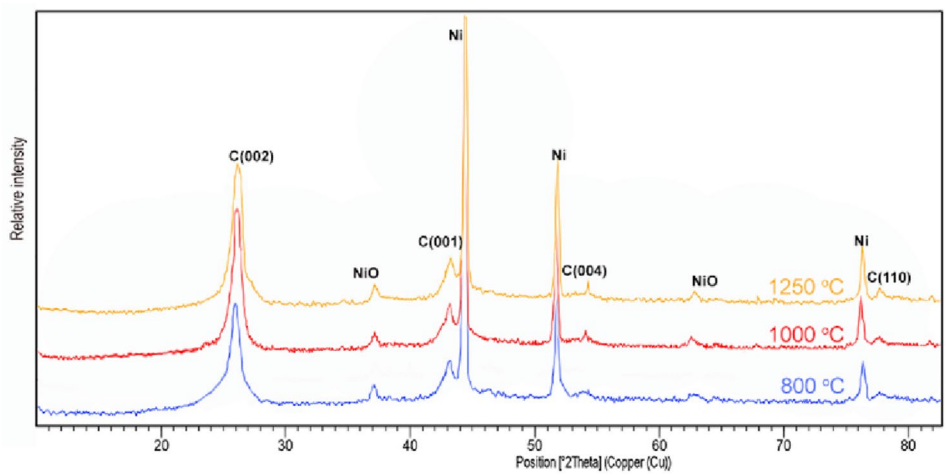

Fig. 3 XRD patterns of PRN-6 sample fired at different temperatures

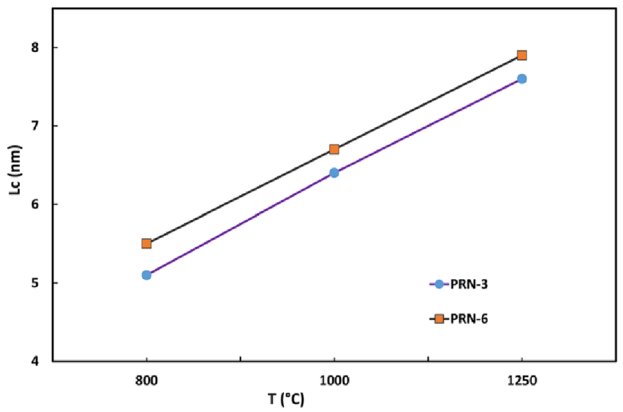

Fig. 4 Crystallite size of PRN-3 and PRN-6 samples fired at different temperatures

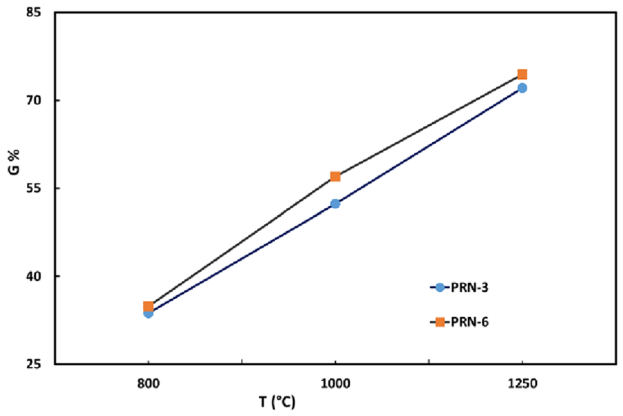

Fig. 5 Graphitization level of PRN-3 and PRN-6 samples fired at different temperatures

graphitization percentage are increased. In general, by examining the results of this test, it can be said that using a nickel-containing additive, the graphitization temperature of carbon resulting from the pyrolysis of phenolic resin is reduced. So that at a temperature of 800 °C for PRN-3 and PRN-6 samples, 33.72% and 34.88% of amorphous carbon have been graphitized, respectively, which has reached 74.41% by increasing curing temperature to 1250 °C in PRN-6 samples, which is considerable. Comparing the results of PRN-3 and PRN-6 samples at different temperatures, it is observed that adding more nickel-containing additives gives better results. In PRN-6 samples, the graphitization percentage ($G\%$) and also the size of crystallites (L_C) is higher than PRN-3 samples at similar temperatures, which indicates a better impact.

3.2 Microstructural observation by FESEM and HRTEM

Figure 6 shows an electron microscope image of a PR cured sample at 1200 °C. As shown in the figure, the PR samples have a homogeneous amorphous structure that has no effect on graphitization and crystalline structure formation.

Figures 7, 8 and 9 show PRN-3 sample images and Figs. 10, 11 and 12 show PRN-6 sample images cured at 800, 1000, and 1250 °C. In PRN-3 and PRN-6 samples cured at 800 °C (Figs. 7 and 10), the microstructural morphology began to change and the carbon microstructure was somewhat non-amorphous and tended toward the onion structure and carbon shells. This structure may normally occur in phenolic resins at temperatures above 2000 °C, but it is reduced below 1000 °C with the addition of nickel nanoparticles [28]. The progression of graphitization in this onion structure is significant and reaches about 33.72 and 34.88% respectively, according to XRD results (for PRN-3 and PRN-6 samples). By increasing the curing temperature to 1000 and 1250 °C for PRN-3 and PRN-6 samples, the amount of graphitized structure is increased. The formation of carbon nanotubes at these temperatures is noticeable as the amount of nanotubes formed increases and also their size becomes larger and their density is increased in the matrix.

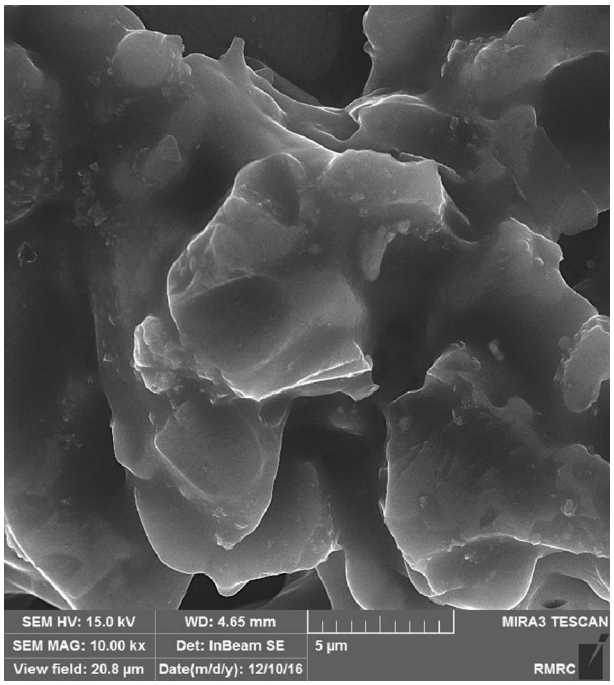

Fig. 6 FESEM image of PR sample fired at 1200 ℃

The formed carbon nanotubes are about 20–60 nm thick and reach more than a few micrometers in length. As shown in the images, the structure is completely hollow and the wall thickness of the formed nanotubes is about 10 nm. In other words, about 30 layers of graphene together form the carbon nanotube wall in these samples.

As can be seen in the figures, a diffraction pattern has been taken from the samples to confirm the XRD results. The diffraction patterns prepared from the samples indicate 4 loops that represent the (002), (100), (004), and (110) crystalline planes which indicate the formation of graphite structure in the samples with the aid of nickel nanoparticles obtained from the nickel-containing additive. The results of the diffraction patterns are in accordance with the XRD results. The loops formed for samples cured at 1000 and 1250 °C, which are specified in the diffraction pattern, are clearer and the number of points composed of crystalline plane is higher. That is, the percentage of graphitization is higher in these samples (Figs. 8d, 9e, 11e and 12e).

Another point that can be seen in the images of PRN-3 and PRN-6 samples is that nickel nanoparticles are formed at one end of carbon nanotubes, which is probably composed of the decomposition of nickel nitrate during the curing process. The growth of nanotubes begins with the formation of a graphite layer around these nanoparticles and continues in a hollow shape (Figs. 8a, 9c and 12c). The shape of nickel nanoparticles is spherical and quasi-oval, which vary between 40 and 200 nm. However, in some cases the nickel particles are agglomerated and larger dimensions are observed (Fig. 9a).

According to the presented microstructural images, it is clear that with increasing the percentage of nickel-containing

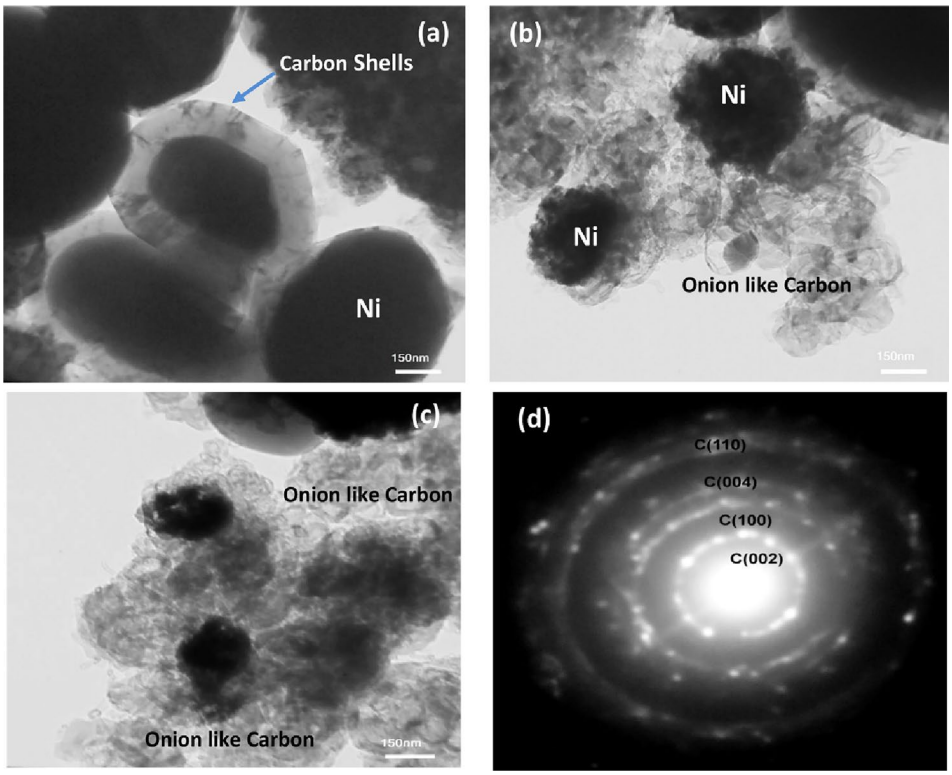

Fig. 7 HRTEM image and diffraction pattern of PRN-3 sample fired at 800 ℃

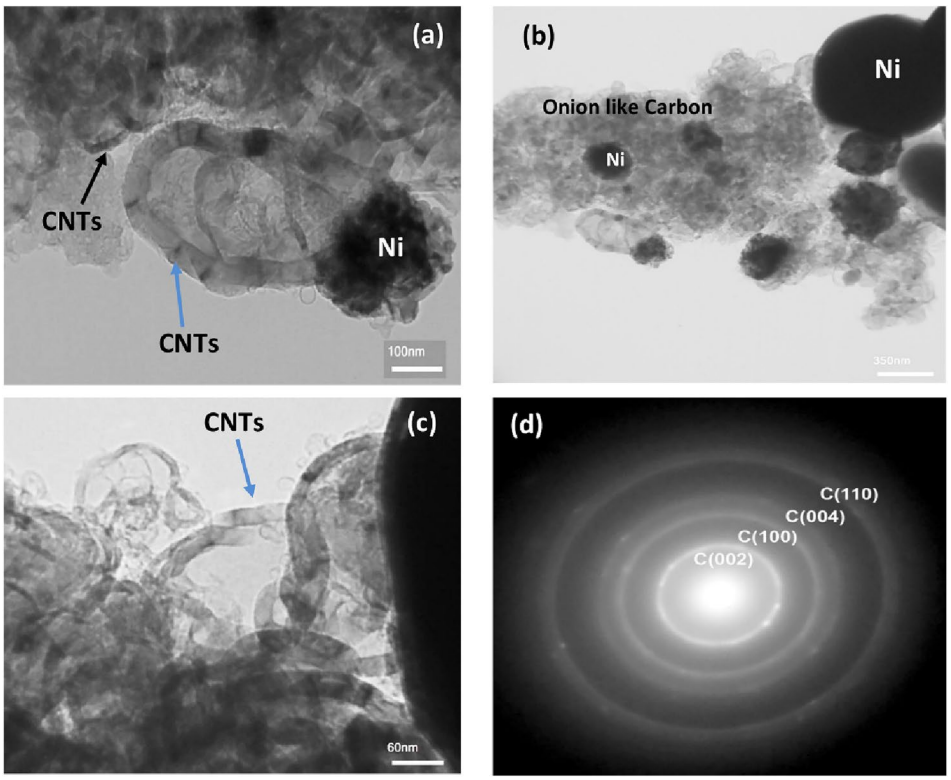

Fig. 8 HRTEM image and diffraction pattern of PRN-3 sample fired at 1000 ℃

additive and curing temperature, the percentage of graphitization is increased, which is observed both in the density of onion skin particles and in the amount and size of carbon nanotubes. In general, it can be said that by increasing the percentage of nickel-containing additive to 6 wt. % and varying the curing temperature from 800 to 1000 and 1200 °C, the morphology of the samples has changed significantly.

3.3 Modified phenolic resin graphitization process

3.3.1 Transition metals selection and mechanism of effect

According to research, the best catalysts utilized in this regard include some of the transition metals. Elements such as Ni are catalytic metals that have the ability to accelerate and facilitate graphitization of amorphous carbon resulting from the pyrolysis of phenolic resins and the formation of carbon nanotubes as well as the formation of ceramic fibers in the bulk of carbon-containing refractories [29, 30]. The reasons for choosing these metals can be described as follows.

1. To select a metal with catalytic capability in the bulk of a carbon-containing refractory, it should be examined whether the oxide compounds of these metals can be reduced by carbon or not? Examination of the Ellingham diagram indicates that the Ni metal is higher than carbon and CO. Given that in the Ellingham diagram, the lower elements can reduce the oxide of the higher elements, then the oxide of this metal can be reduced by carbon and CO [31].

2. The mechanism of formation of carbon nanotubes using metal catalysts is such that during the heating process of the samples, first the adsorption of carbon or carbon-containing compounds resulting from the decomposition of the resin to the surface of the catalytic metal oxide occurs. Then reduction of catalytic metal oxide and in situ formation of nanometals, carbon penetration into nanometals, carbon saturation in nanometals, deposition, and nucleation of graphite layers around nanometals and finally growth of graphite layers in the form of onion, bamboo and carbon nanotube structure and the repetition of this cycle are performed through three mechanisms: solid vapor (VS), vapor–solid–liquid (VLS) and solid–liquid–solid (SLS). One of the necessary conditions in this process is the solubility of carbon in the catalytic metal. However, the amount of this solubility must be very limited to saturate very quickly and precipitate carbon [25]. Examination of the Ni–C binary equilibrium diagram shows that [32] carbon has a very limited solubility region with nickel that can be rapidly saturated and precipitate as a crystalline structure. However, in general, the mechanism of graphitization of amorphous carbon resulting from pyrolysis of phenolic resin due to the formation of catalytic nanoparticles is often similar, and the mechanism of this phenomenon has been explained in our previous research in detail [25].

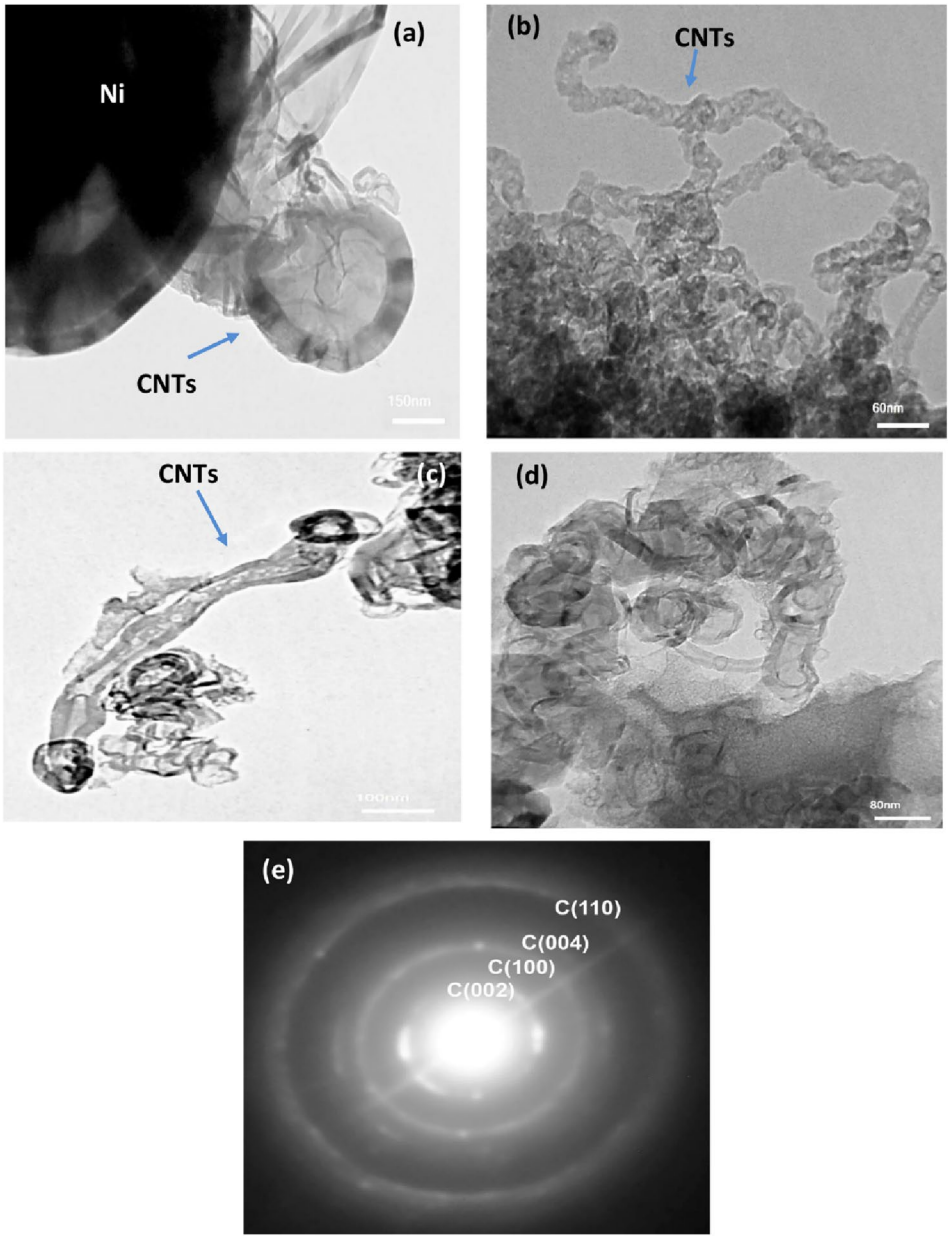

Fig. 9 HRTEM image and diffraction pattern of PRN-3 sample fired at 1250 ℃

3.3.2 In situ formation of nano-Ni, modified carbon and thermodynamic discussion

Nickel nitrate is a raw material that contains the nickel and is gradually transformed to nickel oxide during reactions 3–6 in the heating and preparation process of research samples [33].

$$Ni(NO_3)_2.9H_2O \rightarrow Ni(NO_3)_2.2H_2O + 7H_2O \quad (3)$$

$$H_2O_{(l)} \rightarrow H_2O_{(v)} \quad (4)$$

$$Ni(NO_3)_2.2H_2O \rightarrow 1/3Ni(OH)_2.2Ni(NO_3)_2.2H_2O + 2/3HNO_3 + 2/3H_2O \quad (5)$$

$$1/3Ni(OH)_2.2Ni(NO_3)_2.2H_2O \rightarrow NiO + 4/3NO_2 + 1/3O_2 + H_2O \quad (6)$$

CO, CO_2, H_2, H_2O, CH_4, and C_2H_6 gases are formed in the system during heating of phenolic resin samples. Among the available gases, CO, H_2, and CH_4, can often reduce nickel oxide, and eventually nickel metal is formed in situ according to reactions 7–10 [31, 34].

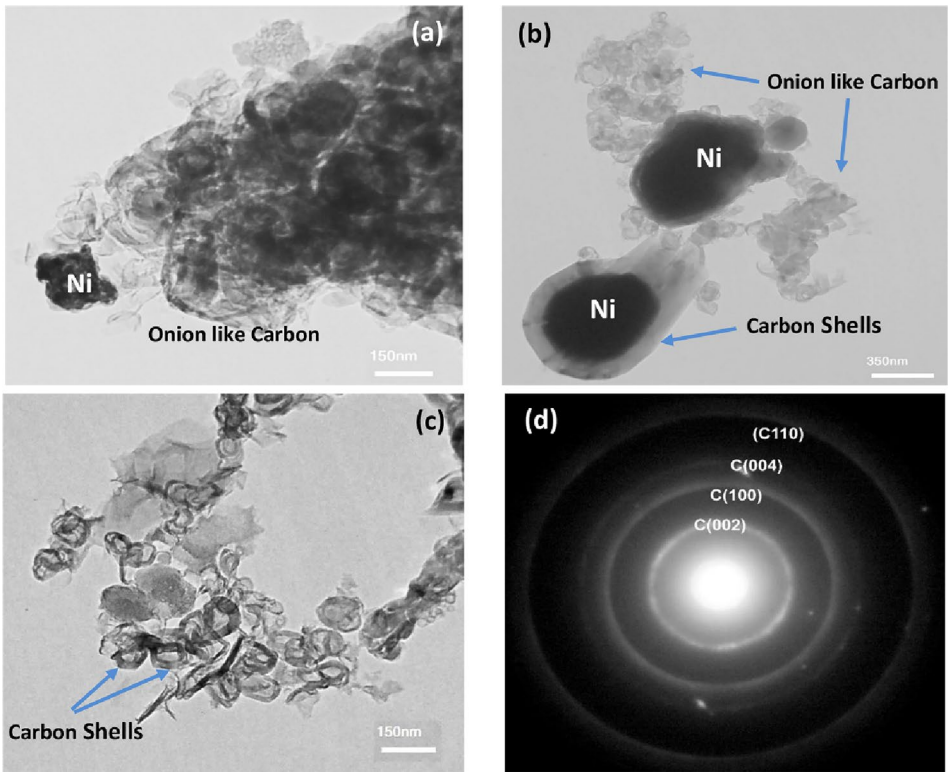

Fig. 10 HRTEM image and diffraction pattern of PRN-6 sample fired at 800 ℃

$$NiO + CO = Ni + CO_2 \qquad \Delta G^\circ = -48,074 + 1.59T(J) \tag{7}$$

$$NiO + C = Ni + CO \qquad \Delta G^\circ = 122,632 - 172.882T(J) \tag{8}$$

$$NiO + H_2 = Ni + H_2O \qquad \Delta G^\circ = -12,092 - 30.42T \tag{9}$$

$$NiO + CH_4 = Ni + CO + 2H_2 \qquad \Delta G^\circ = 53,513 + 51.254 \log T - 238.23T(J). \tag{10}$$

In the curing process, phenolic resin samples are created according to the reducing atmosphere and in the presence of carbon and oxygen, CO, CO_2, and O_2 gases will be in equilibrium through reactions 11–13 [31, 34].

$$2C_{(s)} + O_{2(g)} = 2CO_{(g)} \qquad \Delta G^\circ = -223,426 - 175.3T(J) \tag{11}$$

$$C_{(s)} + O_{2(g)} = CO_{2(g)} \qquad \Delta G^\circ = -394,133 - 0.84T \tag{12}$$

$$2CO_{(g)} + O_{2(g)} = 2CO_{2(g)} \qquad \Delta G^\circ = -564,840 + 173.62T \tag{13}$$

As can be seen, the reactions 11–13 are exothermic, i.e. the above oxidation reactions start at low temperatures. In the presence of solid carbon (graphite and carbon from phenolic resin) and CO_2, another reaction (reaction 14) occurs that is very likely in the reduction atmosphere, called the Boudouard reaction [31, 34].

$$CO_{2(g)} + C_{(s)} = 2CO_{(g)} \qquad \Delta G^\circ = 170,700 - 174.5T(J). \tag{14}$$

Reaction 14 shows an equilibrium between CO and CO_2 in the presence of solid carbon. This reaction is exothermic and is more likely to take place at temperatures above 900 ℃ and form CO. Since the activation energy is very high, this energy cannot be provided at low temperatures, and, therefore, carbon is precipitated. Therefore, it can be said that with the reducing cure atmosphere, at low temperatures, CO_2 gas and solid carbon, and at high temperatures, CO gas will often react with the components. Now, after a relative study of the atmosphere resulting from carbon and its compounds and possible reactions, we will examine the reactions of the components of the research composition during curing in the reducing atmosphere.

Research shows that the presence of nickel nanoparticles plays a catalytic role in the Boudouard reaction and

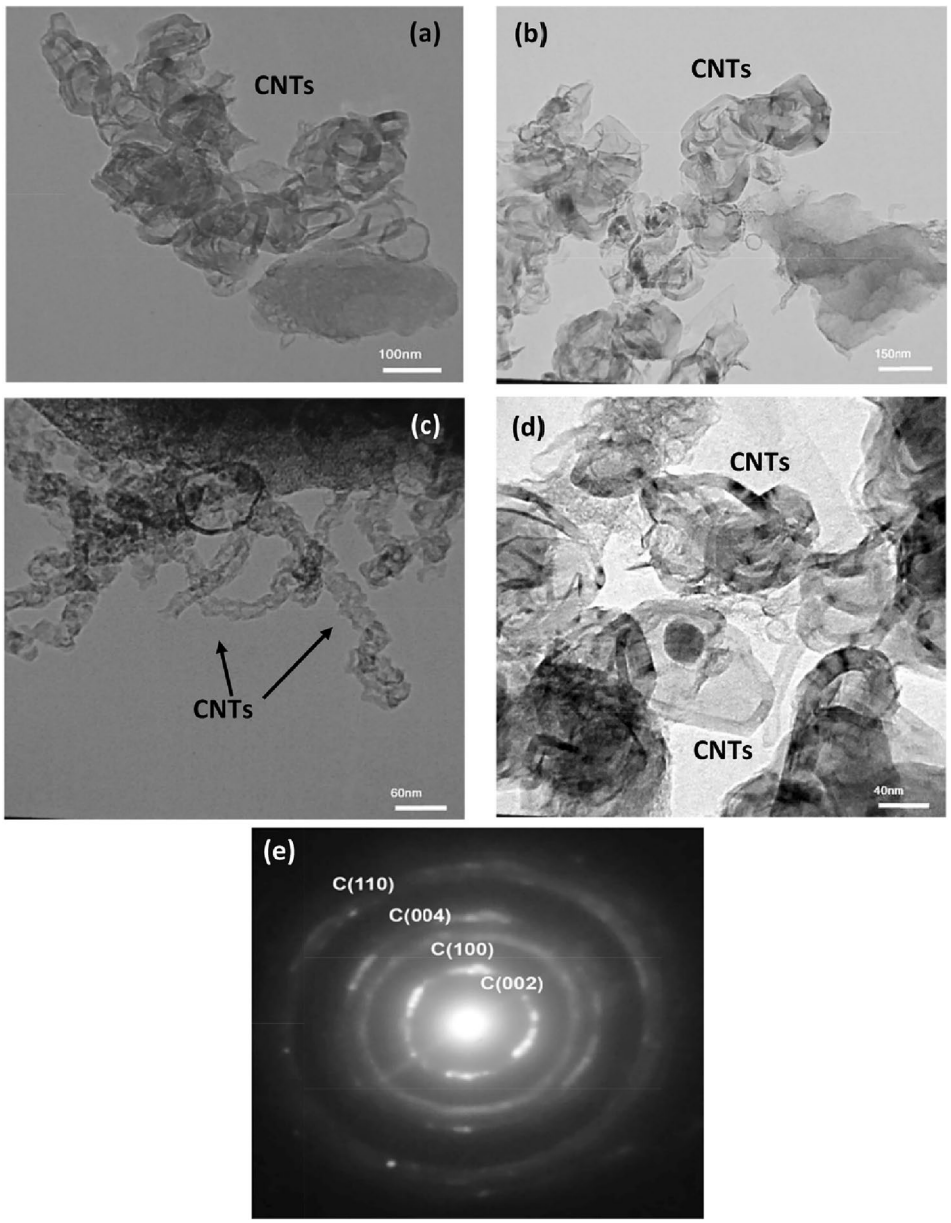

Fig. 11 HRTEM image and diffraction pattern of PRN-6 sample fired at 1000 ℃

accelerates this reaction [35, 36]. In examining the reason for the influence of Ni nanoparticles in the process of this reaction, it should be said that with the presence of carbon in the system, reaction 14 (Boudouard) is inevitable. According to the thermodynamic conditions, the Boudouard reaction takes place more in $CO+CO_2$ gas mixture with increasing temperature from about 900 °C onwards. For a gaseous mixture of CO and CO_2 at atmospheric pressure and in equilibrium with solid carbon, the changes in $\frac{P_{CO}}{P_{CO_2}}$ in terms of temperature are given in Fig. 13, i.e. as the temperature increases [31, 34], reaction 14 moves toward CO production.

With the presence of nickel oxide in the composition, part of the CO produced in the Boudouard reaction can be used to perform reaction 7 and reduce nickel oxide. Given that in the Boudouard reaction, CO_2 must be combined with C to produce CO, more CO consumption means that the Boudouard reaction must advance more and it will be accelerated. Since the produced CO is needed to reduce nickel oxide and is consumed in reaction 7 [31, 34], this cycle is constantly repeated and performed, and thus it can be said that Ni nanoparticles will have a catalytic effect on these reactions.

On the other hand, at temperatures above 750 °C, in addition to increasing the amount of CO, the amount of H_2 available in the furnace atmosphere is also increased

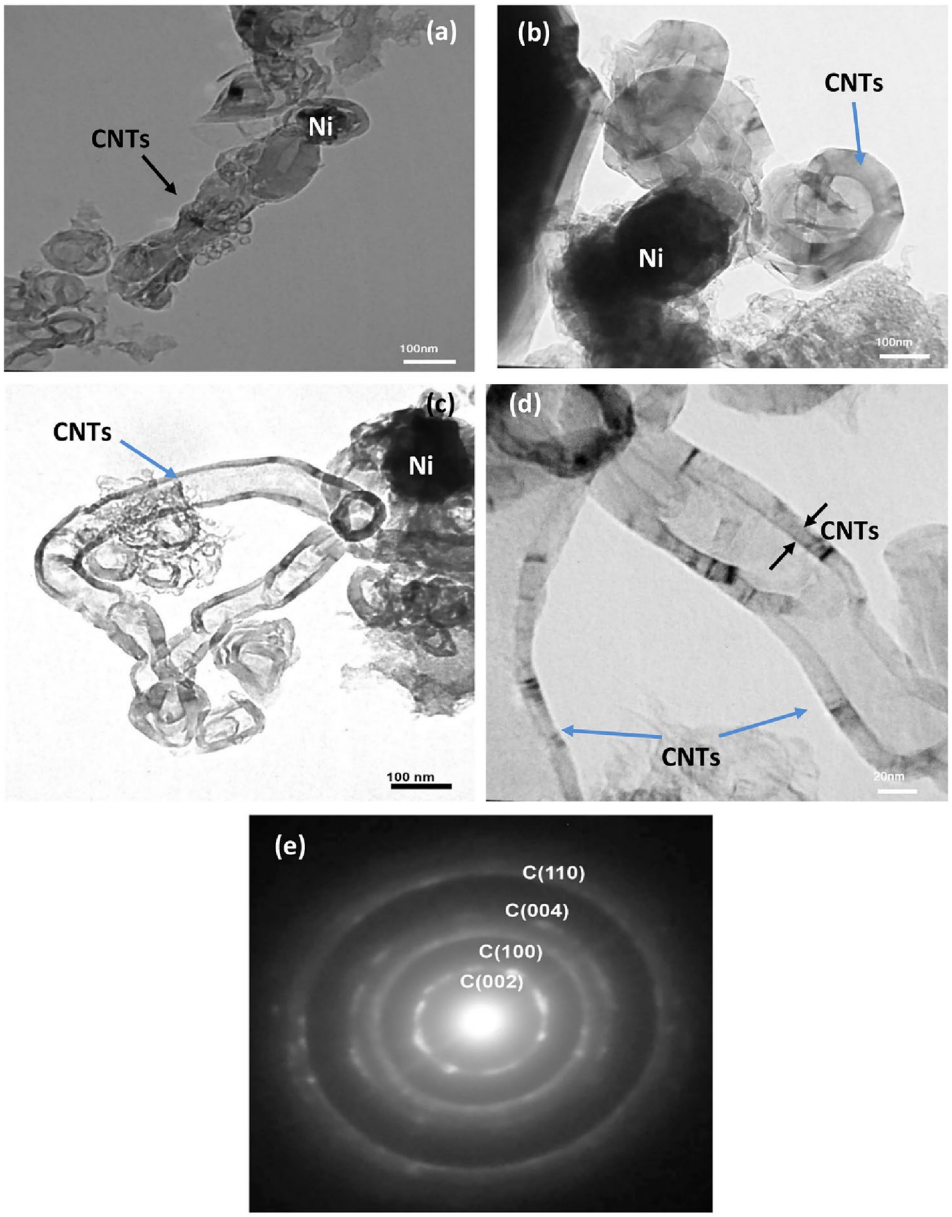

Fig. 12 HRTEM image and diffraction pattern of PRN-6 sample fired at 1250 ℃

using catalytic elements such as nickel. This increase is achieved by breaking the bond of hydrocarbons such as CH_4. Therefore, it can be said that with the formation of nickel in the composition, the percentage of reduction of nickel oxide also increases, and this effect is due to the breakdown and modification of the hydrocarbon structure and the acceleration of reactions 15 and 16.

$$CH_4(g) + CO_2(g) = 2CO(g) + 2H_2(g)$$
$$\Delta G^{\circ} = 239,819 - 51.254 \log T - 109.15T \text{ (J)} \quad (15)$$

$$CO(g) + H_2O(g) = CO_2(g) + H_2(g)$$
$$\Delta G^{\circ} = -71,965 + 64T \quad \text{(J)}. \quad (16)$$

Therefore, it can be said that as a result of these reactions, the amount of reducing gases H_2 and CO increases and as a result, the reduction percentage in nickel oxide increases with increasing time and temperature. Therefore, with the production of Ni nanoparticles, in addition to Ni causing graphitization and preparation of crystalline carbon structures, it also has a positive and catalytic effect on the reduction process of nickel oxide in the system [35, 36]. A schematic view of this process is shown in Fig. 14.

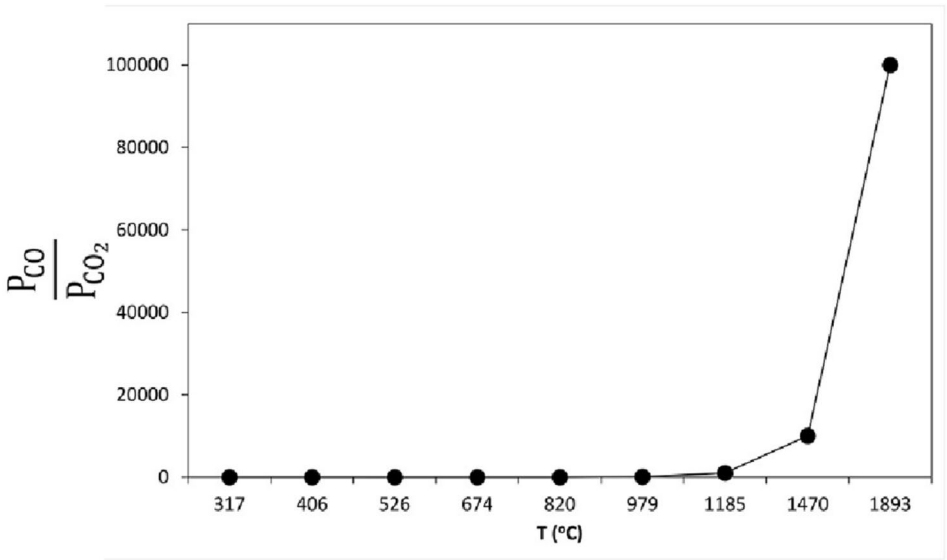

Fig. 13 $\frac{P_{CO}}{P_{CO_2}}$ against temperature

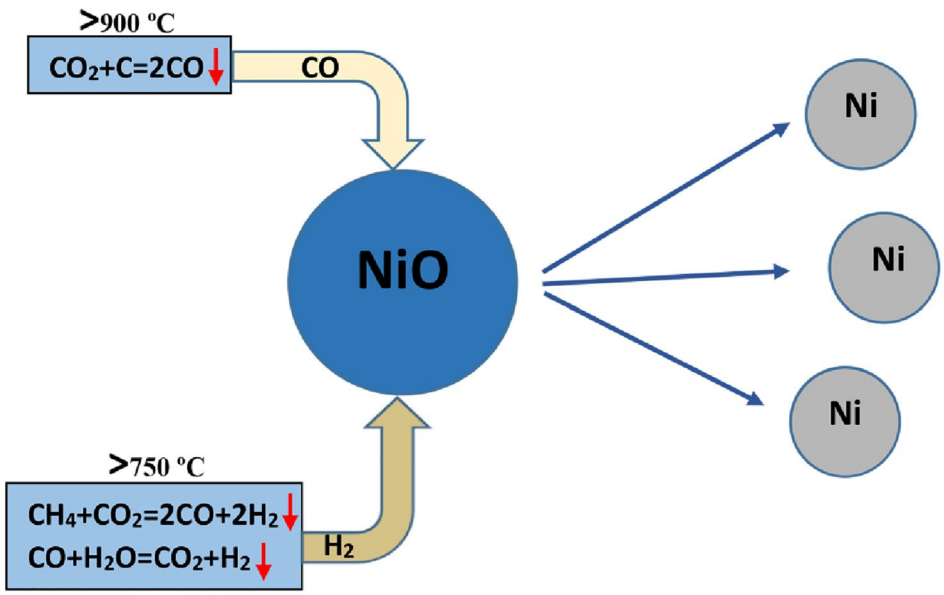

Fig. 14 The schematic of the Ni catalytic effect on H_2 and CO formation

The properties of formed nickel nanoparticles can be influential in the amorphous carbon graphitization process resulting from the pyrolysis of phenolic resins. Thus, when the nickel particle size is smaller (Figs. 8a, 11d and 12c), morphology improvement and increased growth of carbon nanotubes are observed, and where agglomeration occurs (Figs. 7a, 8b, 9a and 10b), carbon does not grow in tube form. Due to the effect of nanoparticle size at the melting temperature, this effect needs to be carefully studied. The relationship between particle size reduction and melting point can be calculated through Eq. 3. This relationship shows that by reducing the particle size to nanoscale, the melting point is significantly reduced [37].

$$\Delta T = \frac{2\gamma MT}{r\rho Q}. \tag{17}$$

In this relation Q is the Moore latent heat of fusion, γ is the surface tension, M is the molecular mass, T is the melting point, r is the particle diameter and ρ is the density.

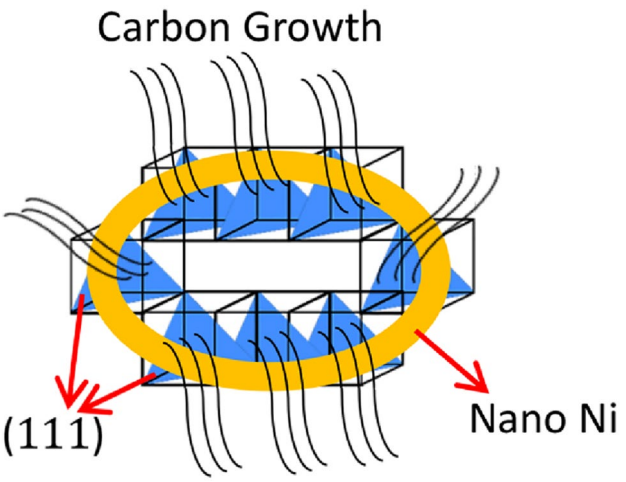

Fig. 15 The suggested schematic for growthing of graphitized carbon from saturated Ni

For example, to calculate this parameter for nickel nanoparticles with a particle diameter of 40 nm:

$$\Delta T = \frac{2 \times \left(1.769 \frac{\mathrm{j}}{\mathrm{m}^2}\right) \times \left(58.69 \frac{\mathrm{g}}{\mathrm{mol}}\right) \times \left(1728 o_k\right)}{\left(40 \times 10^{-9}\ \mathrm{m}\right) \times \left(7.81 \times 10^6 \frac{g}{\mathrm{m}^3}\right) \times \left(17,480 \frac{\mathrm{j}}{\mathrm{mol}}\right)} = 65.7.$$

That is, by reducing the dimensions of nickel metal to 40 nm, its melting point decreases to 65.7 °C and reaches approximately 1389 °C. On the other hand, according to the nickel-carbon diagram, nickel has a eutectic with carbon at a temperature of about 1326 °C, which according to the above calculations, by reducing the size of the nickel particle, there is a possibility of partial melting around the curing temperature in the research samples.

The most important variable factors based on the conditions in Eq. (17) are the surface tension and the desired particle diameter. Previous research has shown that if the nickel particle size is between 10 and 200 nm, the surface tension of the particle does not change significantly and can be ignored [38]. Therefore, the most important available factor is the particle size. Thus, it can be said that by reducing the size of the nickel particle, the amount of ΔT will be higher in the composition, which means that by reducing the nickel particle size, the melting temperature will further decrease.

A very important point in the growth of carbon nanotubes, which may be influential, is the type of crystalline structure of the transition metal used. Given that the crystalline structure of nickel is FCC and the {111} planes are the densest, then saturated carbon from Ni nanoparticles will precipitate on {111} planes and grow in parallel. Thus, when the carbon in the nickel lattice reaches saturation, it leave the quadrilateral and octahedral nickel empty spaces and precipitates on the denser planes, and then the growth process will continue in the direction parallel to these planes. A schematic of the growth of nickel-saturated carbon with FCC structure is shown in Fig. 15. This phenomenon causes graphite carbon to grow in a certain preferential direction, eventually forming carbon nanotubes.

4 Conclusions

Using a nickel-containing additive (nickel nitrate) during the curing process in the carbon substrate, nickel nanoparticles with a size of about 40–200 nm were formed in the phenolic resin. The results of phase studies (XRD) showed that with the addition of nickel, the graphitization temperature of amorphous carbon resulting from the pyrolysis of phenolic resin was reduced, starting at a temperature of about 800 ºC and reaching 74.41% at a curing temperature of 1250 ºC in samples with 6 wt.% of nickel. As the percentage of nano-nickel additive and curing temperature of the modified resin samples increase, the amount of L_C (crystallite size in c direction) and G% (percentage of graphitization) and in other words the amount of graphitization are increased. The microstructure of crystalline carbon formed in phenolic resin with additive is often in the form of carbon nanoparticles with the onion morphology, carbon shells, and CNTs, which by increasing curing temperature as well as the percentage of nickel additive, the amount and size of carbon nanotubes is increased. Also by decreasing of the nickel particle size, morphology improvement, and increased growth of carbon nanotubes are observed, and where agglomeration occurs, carbon does not grow in tube form. Another thing is that, production of Ni nanoparticles has a positive and catalytic effect on the reduction process of nickel oxide in the system.

Studies have shown that, the important point of the research is that the formation of carbon nanotubes in the composition of modified phenolic resin samples is in the form of carbon layers grown from the surface of nickel particles, through the surface of dense planes in FCC nickel crystal structure (parallel to {111} planes).

Declarations

Conflict of interest The corresponding author (Dr. Hossein Rastegar) is member of Saveh Branch, Islamic Azad University in Iran. We wish to confirm that there are no known conflicts of interest associated with this publication and there has been no significant financial support for this work that could have influenced its outcome.

References

1. Pilato L (2010) Phenolic resins: A century of progress. Phenolic Resins A Century Prog. https://doi.org/10.1007/978-3-642-04714-5
2. Cao L, Li Z, Fan G, Jiang L, Zhang D, Moon WJ, Kim YS (2012) The growth of carbon nanotubes in aluminum powders by the catalytic pyrolysis of polyethylene glycol. Carbon N Y 50:1057–1062. https://doi.org/10.1016/j.carbon.2011.10.011
3. Aneziris CG, Borzov D, Ulbricht J, Suren J, Dern H (2004) Phenolic resins with carbo-resin additions for improved MgO-C refractories. Key Eng Mater 264–268:1767–1770. https://doi.org/10.4028/www.scientific.net/KEM.264-268.1767
4. Ewais M (2004) E, Carbon based refractories. J Ceram Soc Japan 112:517–532
5. Su G, Hr D (2005) The influence of carbon materials on the properties of MgO refractories. Mater Tehnol 39:211–213
6. Imamura R, Matsui K, Takeda S, Ozaki J, Oya A (1999) A new role for phosphorus in graphitization of phenolic resin. Carbon NY 37:261267
7. Bitencourt CS, Pandolfelli VC (2013) Thermosetting resins and the production of carbon containing refractories: theoretic basis and insights for future developments. Cerâmica 59:1–26. https://doi.org/10.1590/S0366-69132013000100002
8. Maldhure AV, Wankhade AV (2017) In-situ development of carbon nanotubes network and graphitic carbon by catalytic modification of phenolic resin binder in Al2O3–MgO–C refractories. J Asian Ceram Soc 5:247–254. https://doi.org/10.1016/j.jascer.2017.04.010
9. Wei G, Zhu B, Li X, Ma Z (2015) Microstructure and mechanical properties of low- carbon MgO–C refractories bonded by an Fe nanosheet-modified phenol resin. Ceram Int 41:3541–3548
10. Li RT, Pan W, Sano M (2002) Catalytic reduction of magnesia by carbon. Key Eng Mater 224–226:563–568. https://doi.org/10.4028/www.scientific.net/KEM.224-226.563
11. Rongt L, Wei P, Sano M, Li J (2003) Catalytic reduction of magnesia by carbon. Thermochim Acta 398:265–267. https://doi.org/10.1016/S0040-6031(02)00324-6
12. Rongti L, Wei P, Sano M (2003) Kinetics and mechanism of carbothermic reduction of magnesia. Metall Mater Trans B 34:433–437. https://doi.org/10.1007/s11663-003-0069-y
13. Yu J, Zhao H, Zhang H, Li J, Ding X (2017) Growth of carbon nanofibers in phenolic resin for carbon-contained refractory using different catalysts. J Nanomater 2017:1–5. https://doi.org/10.1155/2017/4826785
14. Zhu T, Li Y, Jin S, Sang S, Liao N (2015) Catalytic formation of one-dimensional nanocarbon and MgO whiskers in low carbon MgO-C refractories. Ceram Int 41:3541–3548. https://doi.org/10.1016/j.ceramint.2014.11.017
15. Stamatin I, Morozan A, Dumitru A, Ciupina V, Prodan G, Niewolski J, Figiel H (2007) The synthesis of multi-walled carbon nanotubes (MWNTs) by catalytic pyrolysis of the phenol-formaldehyde resins. Phys E Low-Dimens Syst Nanostruct 37:44–48. https://doi.org/10.1016/j.physe.2006.10.013
16. Rastegar H, Bavand-vandchali M, Nemati A, Golestani-Fard F (2019) Phase and microstructural evolution of low carbon MgO-C refractories with addition of Fe-catalyzed phenolic resin. Ceram Int 45:3390–3406. https://doi.org/10.1016/j.ceramint.2018.10.253
17. Zhu B, Wei G, Xiangcheng L, Ma Z, Wei Y (2014) In- situ catalytic growth of MgAl2O4 spinel Whiskers in MgO-C refractories. Int J Mater Res 105:593–598
18. Hu Q, Wang X, Wang Z (2013) Preparation of graphitic carbon nanofibres by in situ catalytic graphitisation of phenolic resins. Ceram Int 39:8487–8492. https://doi.org/10.1016/j.ceramint.2013.02.081
19. Wang J, Deng X, Zhang H, Zhang Y, Duan H, Lu L, Tian L, Song S, Zhang S (2016) Synthesis of carbon nanotubes via Fe-catalyzed pyrolysis of phenolic resin. Phys E Low-Dimens Syst Nanostruct 86:24–35
20. Kovalevski VV, Safronov AN (1998) Pyrolysis of hollow carbons on melted catalyst. Carbon NY 36:963–968. https://doi.org/10.1016/S0008-6223(97)00223-6
21. Tzeng SS (2006) Catalytic graphitization of electroless Ni-P coated PAN-based carbon fibers. Carbon N Y 44:1986–1993. https://doi.org/10.1016/j.carbon.2006.01.024
22. Luz AP, Renda CG, Lucas AA, Bertholdo R, Aneziris CG, Pandolfelli VC (2017) Graphitization of phenolic resins for carbon-based refractories. Ceram Int 43:8171–8182. https://doi.org/10.1016/j.ceramint.2017.03.143
23. Darban S, Kakroudi MG, Vandchali MB, Vafa NP, Rezaei F, Charkhesht V (2020) Characterization of Ni-doped pyrolyzed phenolic resin and its addition to the Al2O3–C refractories. Ceram Int 46:20954–20962. https://doi.org/10.1016/j.ceramint.2020.05.153
24. Bitencourt CS, Luz AP, Pagliosa C, Pandolfelli VC (2015) Role of catalytic agents and processing parameters in the graphitization process of a carbon-based refractory binder. Ceram Int 41:13320–13330. https://doi.org/10.1016/j.ceramint.2015.07.115
25. Rastegar H, Bavand-vandchali M, Nemati A, Golestani-Fard F (2018) Catalytic graphitization behavior of phenolic resins by addition of in situ formed nano-Fe particles. Phys E Low-Dimens Syst Nanostruct 101:50–61. https://doi.org/10.1016/j.physe.2018.03.013
26. Jiang G, Goledzinowski M, Comeau FJE, Zarrin H, Lui G, Lenos J, Veileux A, Liu G, Zhang J, Hemmati S, Qiao J, Chen Z (2016) Free-standing functionalized graphene oxide solid electrolytes in electrochemical gas sensors. Adv Funct Mater 26:1729–1736. https://doi.org/10.1002/adfm.201504604
27. Boquan Z, Guoping W, Xiangcheng M, Lieying W, Ying (2013) Structure evolution and oxidation resistance of pyrolytic carbon. In: Unitcer 2013, pp 985–990
28. Okabe K, Shiraishi S, Oya A (2004) Mechanism of heterogeneous graphitization observed in phenolic resin-derived thin carbon fibers heated at 3000 °C. Carbon N Y 42:667–669. https://doi.org/10.1016/j.carbon.2003.11.018
29. Zhao M, Song H (2011) Catalytic graphitization of phenolic resin. J Mater Sci Technol 27:266–270. https://doi.org/10.1016/S1005-0302(11)60060-1
30. Luo M, Li Y, Sang S, Zhao L, Jin S, Li Y (2012) In situ formation of carbon nanotubes and ceramic whiskers in Al2O3–C refractories with addition of Ni-catalyzed phenolic resin. Mater Sci Eng A 558:533–542. https://doi.org/10.1016/j.msea.2012.08.044
31. Gaskell DR (2008) Introduction to the thermodynamic of materials. Taylor & Francis Publication, Berlin
32. Kubaschewski O (1982) IRON-Binary phase diagrams. Springer Science and Business Media, LLS
33. Gadalla AM, Yu HF (1991) Thermal behaviour of Ni(II) nitrate hydrate and its aerosols. J Therm Anal 37:319–331. https://doi.org/10.1007/BF02055934
34. Kubaschewski CO, Alcock F (1979) Metallurgical thermo-chemistry, 5th edn. Oxford Pergamon Press
35. Sutton D, Kelleher B, Ross JR (2001) Review of literature on catalysts for biomass gasification. Fuel Process Technol 73:155–173
36. Chan FL, Tanksale A (2014) Review of recent developments in Ni-based catalysts for biomass gasification. Renew Sustain Energy Rev 38:428–438. https://doi.org/10.1016/j.rser.2014.06.011

37. Zhu BQ, Wei GP, Li XC, Ma Z, Wei Y (2014) Preparation and growth mechanism of carbon nanotubes via catalytic pyrolysis of phenol resin. Mater Res Innov 18:267–272. https://doi.org/10.1179/1433075X13Y.0000000125
38. Zhao X, Xu S, Liu J (2017) Surface tension of liquid metal: role, mechanism and application. Front Energy 11:535–567. https://doi.org/10.1007/s11708-017-0463-9